Suppression of Capillary Instability of a Polymeric Thread via Parallel Plate Confinement

Younggon Son,[†,⊥] Nicos S. Martys,[‡] John G. Hagedorn,[§] and Kalman B. Migler*[,†]

Polymers Division, Building Materials Division, and Mathematical and Computational Sciences Division, NIST, 100 Bureau Dr., Gaithersburg, Maryland 20899

Received March 28, 2003; Revised Manuscript Received May 24, 2003

ABSTRACT: We investigate the stability of a polymer thread imbedded in a matrix that is confined between two parallel plates. Utilizing a combination of experiments, numerical simulations (lattice−Boltzmann), and surface area calculations, we find substantial deviations from the classical results when the diameter of the thread (D_0) is comparable to the height (H) of the matrix. We find three regimes as a function of H/D_0: For $H/D_0 \gtrsim 3$, the thread breaks up into droplets through a finite wavelength axisymmetric capillary instability as described by Rayleigh and Tomotika. For $1.3 \lesssim H/D_0 \lesssim 3$, the effects of the confinement are felt; the shape becomes nonaxisymmetric, the early-stage growth rate decreases, and the wavelength increases. For sufficiently low H/D_0, we observe that the thread is stable with respect to the capillary instability over the experimental time scales. The simulations qualitatively agree with the experiments and reveal that while the shape of the growing bulges is nonaxisymmetic, the narrowing necks are circular. A simple surface area consideration then shows that as the wall-induced asymmetry of the fluctuation increases, the minimally unstable wavelength increases and eventually diverges.

Introduction

It is well-known that a long liquid thread surrounded by an immiscible liquid matrix exhibits sinusoidal distortions, which grow and cause the thread to break up into a row of smaller droplets.[1,2] For example, in polymer blending, threads are formed by flow, and their subsequent disintegration occurs in either the presence or absence of the flow.[3] Thus, a fundamental understanding of this phenomenon is important to predict the size and morphology of the final polymer blends.

The original studies by Rayleigh and Tomotika concern the case where a fluid thread is surrounded by another fluid of infinite extent. As discussed below, a linear stability analysis shows that the thread is unstable because fluctuations for which $\lambda > 2\pi R_0$ grow exponentially, where λ is the wavelength of a given fluctuation and R_0 is the initial thread radius. Recent progress in this area stems from the construction of linear stability analyses for more complex cases, such as when the interface between the immiscible fluids is covered with an insoluble surfactant,[4,5] or to consider the effects of elasticity at the interface.[6] These cases are also relevant to bioengineering applications.

The effects of experimental geometry on the Rayleigh−Tomotika instability can be profound. In the two-dimensional case where the stability of a flat ribbon is investigated, it was theoretically shown by Miguel[7] that thermal fluctuations decay; intuitively, this can be understood by the observation that the fluctuations cause an increase in surface area. The case of a liquid annular coating on the inside or outside of a cylinder was investigated by Goren.[8] Newhouse and Pozrikidis[9] studied numerically the case where the thread of radius R_0 encompasses a matrix fluid which is confined to a tube of radius R_t. In the limit $R_0/R_t \ll 1$ they recover the results of Rayleigh−Tomotika; as R_0/R_t increases, the thread still breaks into an array of alternating large and small droplets and the dominant wavelength of instability does not change significantly, but the amplitude growth slows down significantly and the shape of the axisymmetric fluctuation changes. When $R_0/R_t > 0.82$ the thin outer layer evolves into an array of lobes or collars. Their case represents confinement in an axisymmetric geometry.

In a recent paper by Migler,[10] a combination of simple shear and confinement between parallel plates was utilized to generate threads (called "strings" in that work). Upon cessation of flow, threads of sufficiently large diameter were found to be stable with respect to the capillary instability. That experiment then considers a different geometry from those considered previously: a thread confined between parallel plates, which involves both confinement and nonaxisymmetry. This regime is important because there is great current interest in micro- and nanolength scale technologies in which polymer blends can play an important role,[11,12] but the understanding of the processing of polymer blends when the size of the minor phase is comparable to a sample dimension is poor.

A second application of thread breakup between parallel plates occurs during the measurement of interfacial tension of polymers.[13−16] To ensure that the elastic effect of polymer is negligible in the interfacial tension measurement, the growth rate of the distortion must be sufficiently low because Tomotika's theory assumes that both liquid phases are Newtonian fluids. As the kinetics are inversely proportional to a characteristic length scale, bigger threads are experimentally desirable. However, as the size of the thread increases and becomes comparable to the gap width, the hydrodynamic interaction between the drop and the wall may not be negligible. A study of the thread instability on the confined regime can provide a guide for exact interfacial tension measurement. Finally, our work is relevant to two-phase microfluidics, as it demonstrates

* Corresponding author: e-mail kalman.migler@nist.gov.
† Polymers Division.
‡ Building Materials Division.
§ Mathematical and Computational Sciences Division.
⊥ Current address: Advanced Materials Science & Engineering, Kongju National University, Kongju, Chungnam 314701, S. Korea.

10.1021/ma0343986
Published on Web 06/27/2003

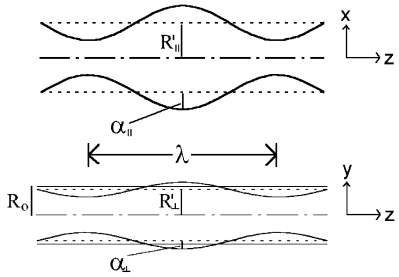

Figure 1. Schematic view of a thread undergoing a nonaxisymmetric capillary instability. The fluid is unconfined in the experimentally observable top view ($x-z$ plane). The side view shows how the matrix fluid is confined in the y direction by parallel plates that are separated by a distance H.

a strategy whereby one may be able to stabilize liquid threads.

In the present study, we examine in detail the effects that occur when the thread diameter is comparable to the gap between two confining parallel plates via a combination of experimental, lattice−Boltzmann (LB) numerical simulations, and surface area calculations. The experimental work demonstrates the basic phenomena of how the confinement acts to inhibit the instability. The lattice−Boltzmann simulations agree qualitatively with the experiments and allow visualization in directions that are experimentally inaccessible. The surface area calculations show that if the confinement causes the thread to grow nonaxisymmetrically (somewhat flattened as depicted in Figure 1), then the critical wavelength increases and the driving force for the instability (the reduction of surface area) decreases. The lattice−Boltzmann simulations validate key assumptions of the surface area calculations.

Background

For the case of a viscous thread in an infinite viscous medium, Tomotika[2] extended Lord Rayleigh's[1] pioneering study to the breakup of Newtonian liquid cylinders in a Newtonian liquid matrix for the case in which no overall flow field is present. Initially, a liquid cylinder of radius $R_0 = D_0/2$ (D_0 is the thread diameter) is subject to thermally induced sinusoidal distortions of arbitrary wavelengths λ. For fluctuations (of amplitude α) and wavelength, λ, there is a decrease in the total interfacial area with increasing $\alpha$for the case $\lambda > 2\pi R_0$. This decrease in area provides the driving force for growth of the instability. The dimensionless wavenumber X is defined by

$$X = \frac{2\pi R_0}{\lambda} \tag{1}$$

There is a critical wavenumber, $X_c = 1$, separating fluctuations that decay ($X > X_c$) from those that grow in time ($X < X_c$). A linear stability analysis shows that in the early-stage growth fluctuations grow exponentially with time:

$$\alpha = \alpha_0 \exp(qt) \tag{2}$$

where α_0 is the initial amplitude and the growth rate of this distortion, q, is given by

$$q = \frac{\sigma\Omega(X,p)}{2\eta_m R_0} \tag{3}$$

where σ is the interfacial tension, η_m is the viscosity of the matrix, p is the thread/matrix viscosity ratio, and R_0 is the initial thread diameter. The function, $\Omega(X,p)$, can be obtained from Tomotika's original paper.[2] For a given viscosity ratio p, there is one dominant wavelength X_m at which the amplitude grows fastest; the distortion having this wavelength consequently leads the thread to break up into droplets.

At first it seems counterintuitive that a fluctuation, which increases the contour length of the thread, can cause a decrease in surface area. The total area of an axisymmetric thread per average unit length is approximately

$$A \cong 2\pi R'\lambda\left[1 + \left(\frac{\alpha\pi}{\lambda}\right)^2\right] \tag{4}$$

in the limit of $\alpha\pi/\lambda \ll 1$. Applying conservation of volume to the distorted thread (which has a circular cross section everywhere) leads to a decrease in the average radius of the thread:

$$R'^2 = R_0^{\,2} - \frac{\alpha^2}{2} \tag{5}$$

Thus, there are two competing effects for the interfacial area: the contour length increase vs the average decrease of the thread radius. It can be seen that for $X < 1$ there is an overall reduction in surface area. Thus, the decrease in surface area is due to the geometry of the thread, namely, the fact that the cross-sectional area scales as r^2. In the present problem we shall see that the confinement causes the fluctuation to grow asymmetrically. Because of the asymmetry, the decrease in interfacial area becomes a weaker effect compared to the increase in contour length; consequently, the wavelength of the fastest growing mode increases while the growth rate is reduced.

Experimental and Numerical Methods

Materials. Two polymers are used in this study. Polyamide-6 (PA-6) was purchased from Polysciences Inc. (M_n = 16 000).[17] Polystyrene (PS) was donated from Dow Chemicals (Styron 666D) **.** The reason for choosing the nylon/PS system is that the nylon thread can be embedding into the PS phase without deforming (or flattening) it. If we had chosen a system such as PS/PMMA or PS/PP, it would be very difficult to embed the thread into the matrix without deforming it because the threads would be soft at the temperature at which PS can flow and vice versa. However, at just below melting temperature of nylon (for example, 200 °C), PS can flow easily and nylon is still hard, allowing the embedding process. Degradation of nylon is not serious because it is fully covered with PS and nylon does not contact oxygen direction; also, the instability process is normally completed within 30 min.

Rheological Measurement. The zero-shear viscosities of the polymers are obtained by measuring the shear viscosity in the range (10^{-2}−5 s^{-1}) in steady-state mode. The polymers used in this study show a Newtonian regime over the shear rate of 10^{-2}−10^{-1} s^{-1}. The rheometer used is an Advanced Rheometric Expansion System (ARES). A parallel plate configuration (diameter = 25 mm) is used with a gap of about 1.0 mm. The temperature for the measurement is 230 °C. The measured zero-shear viscosities of PA-6 and PS are 300 and 1200 Pa·s, respectively, and thus $p = 0.25$.

Experimental Procedure. The observation of the capillary instability is carried out under a similar procedure to that used for the measurement of interfacial tension by the breaking

thread.[14,15] We observe the capillary instability as a function of H/D_0, where H is the gap width and D_0 the initial thread diameter.

Disks of PS in 1 mm thickness and 25 mm diameter are prepared by pressing between two metal plates on a Carver laboratory press at 180 °C. The PA-6 fibers are obtained by drawing from molten pellets at 230 °C obtaining thread diameters ranging from 100 to 300 μm. The fibers are cut to 20 mm length and annealed at 80 °C for about 24 h in a vacuum. An Optical Shearing System (model Linkam CSS 450) connected to a videocassette recorder and to a Zeiss transmission optical microscope is used. This device enables the sample to be sheared and heated simultaneously with various gap widths under microscopic observation.

The fiber of PA-6 is placed between two films of PS. This sandwiched sample is placed in the shearing device under the microscope. At first, the temperature is elevated and maintained at 200 °C for 10 min in order to ensure imbedding without any undesired deformation of the PA-6 fiber (T_m = 216 °C). The gap between the two glass walls is then adjusted very slowly to the desired size range (from 0.4 to 2.5 mm). We have found that the nylon thread remains centered between the two walls. First, the initial thicknesses of the two PS plates are the same, and second, the shear forces during the compression act to keep the thread centered. The position of the thread was confirmed several times by changing the focus of microscope from the bottom wall to the thread and then to the top wall. The temperature is then increased to 230 °C. To perform observations, images from the microscope are recorded onto S-VHS videotape. The observed images of the capillary instability phenomenon are in the directions parallel to the glass wall ($x-z$ plane, top view in Figure 1).

Lattice−Boltzmann Methodology. We utilize a lattice−Boltzmann (LB) method[18−22] to numerically simulate the capillary instability of a confined thread. LB is a computationally efficient approach for modeling multicomponent fluid systems. The approach is to consider a typical volume element of fluid to be composed of a collection of particles that are represented in terms of a particle velocity distribution function at each point in space where fluid particles collide with each other as they move under applied forces. Macroscopic variables such as density and velocity are obtained by taking appropriate moments of the velocity distribution function. It has been shown that this formalism leads to a velocity and density field that is a solution of both the Navier−Stokes and continuity equations. The specific multicomponent LB model utilized for this paper is based on the Shan−Chen approach[22] with further modifications found in Martys and Douglas.[18]

For the present work, we utilize a parallel plate geometry having periodic boundary conditions. A cylindrical thread is introduced, centered between the parallel plates such that its z axis is parallel to the plates. The cylindrical thread is embedded in a second fluid. No-slip boundary conditions are maintained at the fluid/wall interface by using a second-order bounce-back algorithm. To introduce a perturbation to the thread, a small localized body force is applied near the fluid/fluid interface for a few lattice Boltzmann time steps. The widths of the thread in the perpendicular (y) and parallel (x) directions are determined as a function of axial position and time.

Two viscosity ratios were considered. First, we consider the case $p = 1$ (viscous matched) because for computational reasons related to the LB method, significant computer memory can be saved, allowing for much larger simulations than for $p \neq 1$. Here, the system dimension is 800 (in units of lattice spacing) in the z direction and 740 in x. The gap spacing, H, for the three simulations is such that H/D_0 is equal to 2.1, 1.45, and then 1.25 for the three simulations, where $D_0 = 160$. This system size was required in order to have an adequate numerical resolution for the case of $H/D_0 = 1.25$. In a second set of runs we used the same viscosity ratio as the experiments $p = 0.25$ with the following system dimensions: 180 units in z, 88 in x and H, such that $H/D_0 = 2.1$ and 1.4 where $D_0 = 40$. Time is given in the dimensionless quantity qt.

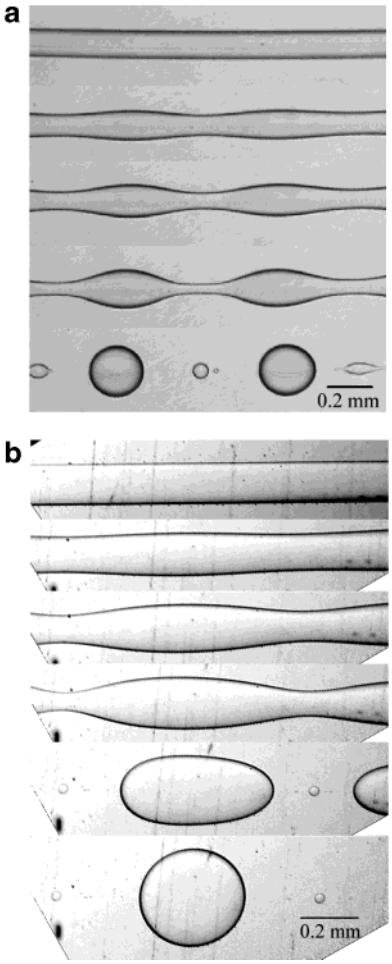

Figure 2. Sinusoidal distortions on a PA-6 thread embedded in a polystyrene matrix. The measurements were performed at 230 °C. Viscosity ratio (p) is 0.25. (a) $H/D_0 = 10.6$; initial thread diameter = 127 μm; the times for subsequent photographs are 0, 471, 542, 615, and 754 s. (b) $H/D_0 = 1.45$; initial thread diameter = 138.4 μm; the times for subsequent photographs are 0, 344, 894, 1073, 1358, and 2315 s.

One important difference between the experiment and the simulation concerns the wavelength of the instability. In the experiment, the thread is essentially free to find the fastest growing wavelength, whereas in the simulation the length of the thread is finite (for reasons of computational resources). The wavelength of the distortion can only take values that are L/n, where L is the length of the simulation box in the z direction and n is an integer. For the case of $n = 1$, then $2\pi R_0/\lambda = 0.7$, which is somewhat larger than what one obtains by considering the fastest growing mode $2\pi R_0/\lambda = 0.59$ at $p = 1$. This discrepancy means that comparisons are qualitative in nature.

Results and Discussion

Experiment. Figure 2 is a typical set of optical micrographs showing the growth of the capillary instability of a PA-6 thread in PS matrix at 230 °C. We present two sets of micrographs. Figure 2A is for the case of a PA-6 thread immersed in a PS matrix where the gap width is much greater than the initial thread diameter ($H \gg D_0$). In Figure 2B, the other case, the thread diameter and gap are of comparable size ($H \approx 1.5\ D_0$). Hereafter, we designate the former case as unconfined and the latter case as moderately confined. In both cases, initially cylindrical threads transform gradually into a row of droplets via an increase in the

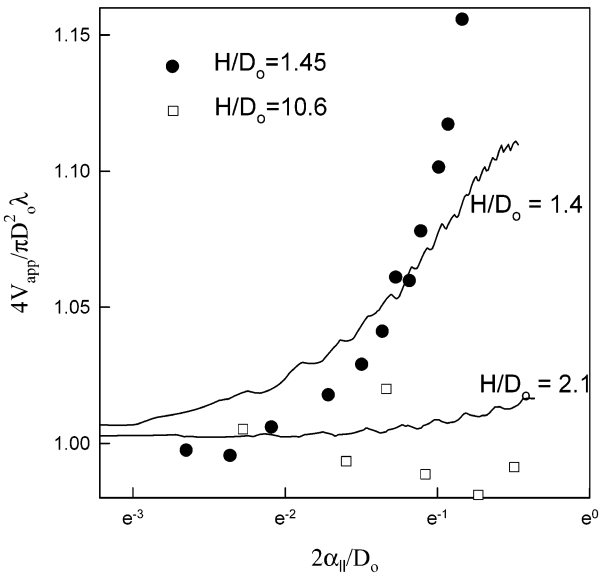

Figure 3. Discrete points represent the normalized apparent volume of the thread, $4V_{app}/(\pi D_0^2\lambda)$, as a function of the relative amplitude of distortion ($2\alpha/D_0$). Apparent volumes of the threads were calculated from the 2D photographs assuming distorted threads are axisymmetrical. Viscosity ratio (p) is 0.25. The standard uncertainty (one standard deviation) is less than 2%. The solid lines are the simulation results (upper: $H/D_0 = 1.4$; lower: $H/D_0 = 2.1$; viscosity ratio, $p = 1$).

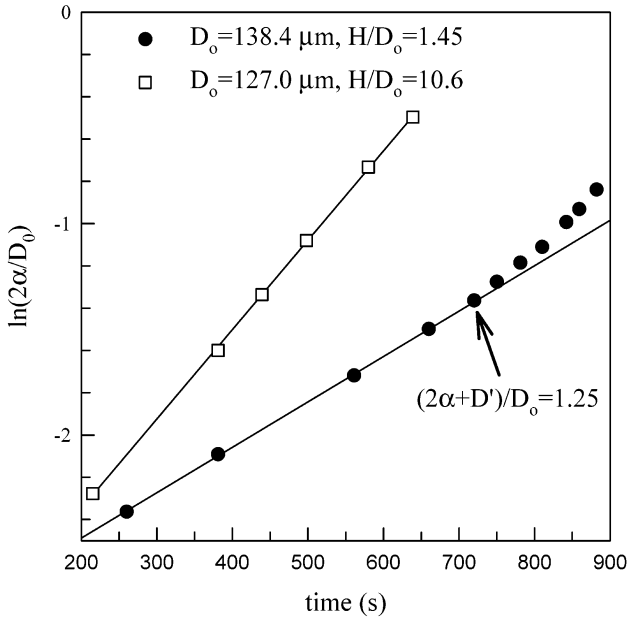

Figure 4. Relative thread distortion amplitude, $2\alpha/D_0$, as a function of time for two different H/D_0 ratios (gap width/initial thread diameter). Viscosity ratio (p) is 0.25. The standard uncertainty (one standard deviation) is less than 3%.

amplitude of a sinusoidal fluctuation. However, the sequence of micrographs immediately reveals significant differences between the two cases. The radius of the final spheres is approximately 2 times larger than that of the original thread (R_0) in the unconfined regime. This is consistent with the predicted radius by volume conservation,[14] i.e., $R_0(1.5\pi/X_m)^{1/3}$. However, that in the moderately confined regime is larger than $2R_0$, and the distance between the droplets is therefore greater than in the unconfined case. Thus, the wavelength of the initial fluctuation in the moderately confined regime is larger than that in the unconfined case, and the final drop shape is a "squashed sphere" because the gap width is smaller than the circle which is observed from the $x-z$ plane. Later, we show that the dimensionless wavenumber of the distortion, $2\pi R_0/\lambda$, is a function of (H/D_0).

To determine whether the confinement causes the thread to grow in a nonaxisymmetric manner, we calculate the dimensionless *apparent* volume of the sinusoidal thread as a function of time. The apparent volume of the sinusoidal thread, V_{app}, is calculated from the fluctuation in the x direction (parallel to the plates) with the assumption that the fluctuation is axisymmetric. This is necessary since we observe the fluctuations in the x direction (refer to Figure 1), but not in the y direction. The dimensionless apparent volume V'_{app} is then obtained by dividing by the volume of the initial thread $V'_{app} = V_{app}/\pi R_0^2\lambda$. If a fluctuation is axisymmetric, then $V'_{app} = 1$, whereas if the fluctuation is greater in the x direction than y, then $V'_{app} > 1$.

Figure 3 is a plot of V'_{app}as a function of amplitude (α), showing that in the unconfined regime V'_{app} is constant within experimental error. The solid lines are the results of a numerical simulation and will be discussed later. This confirms the expected result that when $H \gg D_0$, the fluctuation is axisymmetric. However, in the moderately confined case V'_{app} increases as the instability grows. Note that the deviation from $V'_{app} = 1$ first becomes noticeable when $\alpha/R_0 \approx 0.1$. This occurs well before an axisymmetric surface would impinge on the wall (which occurs at $\alpha/R_0 \approx 0.45$). This result implies that the growth toward the glass wall (perpendicular to the observation plane) in the moderately confined regime is smaller than that in the direction parallel to the observation plane. As the PS matrix between the glass wall and a PA-6 thread is squeezed out as the amplitude grows, the hydrodynamic interaction between the thread and the wall increases. As the distance between the wall and the largest perimeter of the sinusoidal thread decreases by the growth, the hydrodynamic resistance for flow of the matrix phase increases. Therefore, the growth toward the wall is hindered, resulting in the nonaxisymmetric (flattened) sinusoidal thread.

Figure 4 is a plot of relative amplitude ($2\alpha/D_0$) vs time for the same experiment as in Figure 3. For a given run, the straight-line fit to the semilogarithmic plot for the unconfined regime demonstrates the well-known early-stage exponential growth of the fluctuation as a function of time. The situation for the moderately confined regime is different. A straight line for lower H/D_0 (the confined regime) is drawn by a linear regression with the initial five data points. The early-stage growth rate in the confined regime is much slower, even though the initial thread diameters in both cases are similar. At later times ($t > 700$ s), the growth rate increases and becomes comparable to the unconfined case. As indicated in Figure 3, the growth rate toward the glass wall is hindered by the hydrodynamic interaction with the wall. The data points begin to deviate upward from the straight line at about 720 s, which corresponds to the largest diameter of the sinusoidal thread/initial thread diameter ratio of 1.25, which is still smaller than $H/D_0 = 1.45$. As the amplitude grows, the thread becomes more flattened by the hydrodynamic interaction.

Figure 5 is a plot of the scaled growth rate vs H/D_0. The growth rate is the slope of $2R_0 \ln(\alpha/R_0)$ as a function

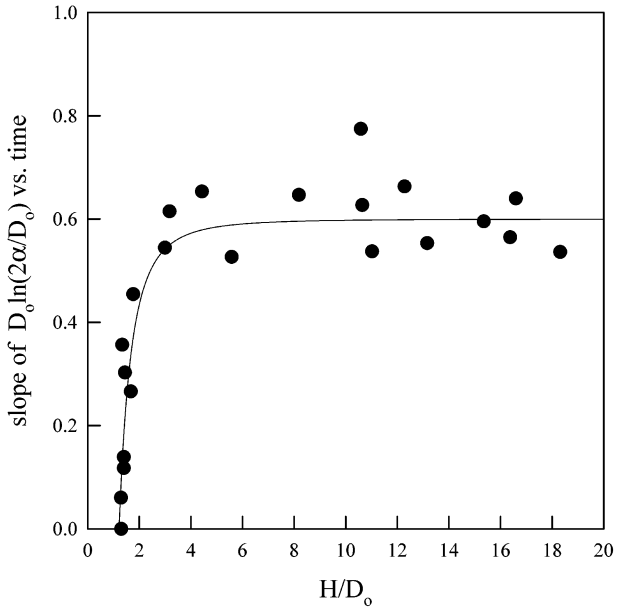

Figure 5. Slope for the plot $\ln(2\alpha/D_0)$ vs time as a function of H/D_0. Viscosity ratio (p) is 0.25. The standard uncertainty (one standard deviation) is less than 10%.

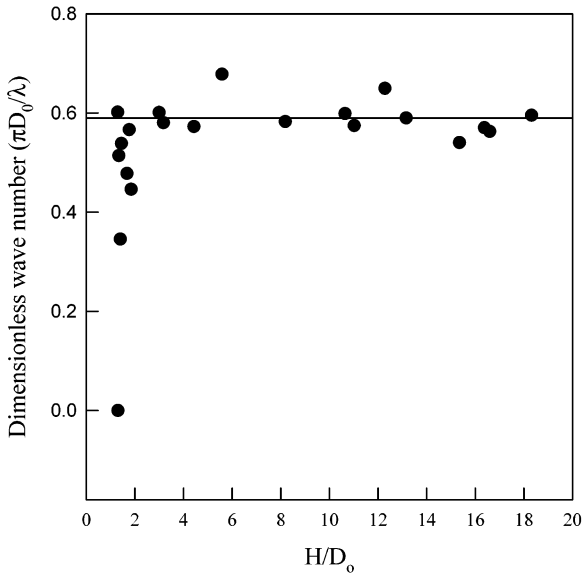

Figure 6. Dimensionless wavenumber vs H/D_0. Viscosity ratio (p) is 0.25. Horizontal line represents theoretical dimensionless wavenumber calculated from Tomotika's theory. The standard uncertainty (one standard deviation) is less than 10%.

of time, as suggested by Tomotika. This slope is directly related to the interfacial tension by eq 3. The slope is constant within the experimental uncertainty for $H/D_0 > 3$; the solid line is drawn to aid the eye. The interfacial tension obtained above for $H/D_0 > 3$ is (5.7 ± 0.49 mN/m). This value is reasonable compared to the values reported elsewhere.[13,16,23,24] However, the slope decreases rapidly for $H/D_0 < 3$. It is reasonable to expect that the growth rate is hindered by the hydrodynamic interaction between the wall and the thread as the thread size increases. One experimental run shows that at $H/D_0 = 1.3 \pm 0.05$ the thread does not show the distortion growth. It maintains its original shape for several hours**.** We refer to this case as strongly confined. This result is consistent with Migler's[10] previously mentioned experimental observation, whereby sufficiently large diameter PDMS threads were stable upon cessation of shear. In that case, the viscosities were matched and $H/D_0 = 0.83 \pm 0.15$. So in the present experiment, where $p = 0.25$, the confinement effect is even stronger, in that thread stabilization occurs for a lesser degree of confinement. In both the present work and the prior PDMS experiment[10] the strongly confined thread is stable over a time scale at least 40 times longer than the unconfined breakup time. Figure 6 plots the dimensionless wavenumber, $2\pi R_0/\lambda$, vs H/D_0. The dimensionless wavenumber is constant within experimental uncertainty for $H/D_0 > 3$. At $H/D_0 < 3$, it decreases.

Lattice−Boltzmann Simulations. We employ lattice−Boltzmann simulations as described in the Experimental and Numerical Methods section in order to gain critical information that is not accessible from the experiments. First, we present results obtained from the $p = 1$ case where three levels of confinement were considered: least-confined ($H/d = 2.1$), moderately confined ($H/d = 1.45$), and strongly confined ($H/d = 1.2$). (The labels unconfined, moderately confined, and strongly confined are used in anticipation of the results.)

Before giving a quantitative analysis of the results, we first present two plots that give a pictorial representation of our observations. Figure 7 shows end-on cross sections of the thread ($x-y$ plane) at the widest and narrowest points that result from the three levels of confinement considered here. For the case of $H/d = 2.1$ (Figure 7A) and the moderately confined case $H/D_0 = 1.45$ (Figure 7B), we show the cross sections when the amplitude of the fluctuation is large, but before actual breakup has occurred. For the strongly confined case (Figure 7C), we show the cross sections at the same two planes as for Figure 7B,C at the last time step of the simulation. We can immediately make three qualitative observations, namely that for the case of $H/D_0 = 2.1$ (the least-confined case) the distortion is axisymmetric, for the confined case it is nonaxisymmetric, and for the strongly confined case it is stable (over the time scale of the simulation.) These observations agree with the experimental results.

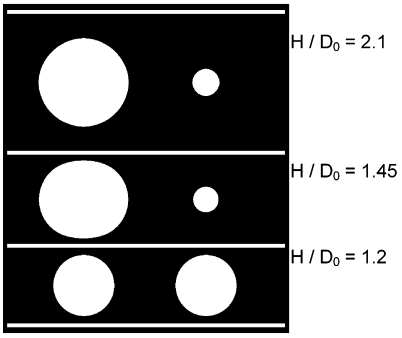

Figure 7. Cross sections of the thread in the $x-y$ plane showing the thread at the planes where it is widest (left side) and narrowest (right sides) for the three levels of the confinement H/D_0 for viscosity ratio (p) = 1. In the top and middle case $H/D_0 = 2.1$ and $H/D_0 = 1.45$, respectively; the threads are shown at times near final breakup, $t = 29$ and 76.2, respectively. For the bottom case of $H/d = 1.2$, $t = 66$, and no growth is observed. Nonaxisymmetric growth is seen in the middle case.

As the kinetics of the moderately confined case is the most interesting, we explore the kinetics of the growth of the fluctuation in further detail in the next three figures. In Figure 8 we show three-dimensional snapshots of the thread as it breaks up. At early times, ($t <$ 100) the thread appears cylindrical, and Figure 8A ($t =$

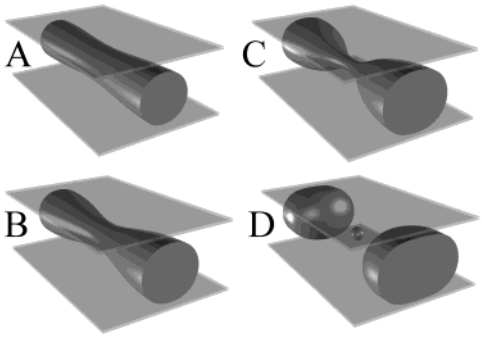

Figure 8. Three-dimensional representation of the moderately confined thread as it breaks up. The times are (A) t = 73.9, (B) 77.1, (C) 78.6, and (D) 80.2 (final breakup).

73.9) shows the structure when the distortion is first apparent by visible inspection. As the breakup proceeds (Figure 8B,C), we observe that the distortion becomes increasingly asymmetric. Note that the asymmetry is observed in the bulge and that the asymmetry begins appearing well before the thread impinges on the wall.

Quantification of the nonaxisymmetric breakup is shown in Figure 9. In these figures, the thick dashed line is the radius of the string as a function of axial position in the y direction (perpendicular to plates), and the solid line is that in the x direction (parallel to the plates). The thin dashed line at 112 indicates the gap thickness of this simulation. Figure 9A−C shows profiles at three times leading to breakup. There are three key points to note. First, the asymmetry occurs even when the amplitude of the distortion is low (Figure 9A). Second, the asymmetry between the x and y directions occurs in the bulge (Z = 200), but not in the neck (Z = 600), a trend that increases in magnitude as the distortion increases (Figure 9B). Third, it is clearly possible to obtain distortions in which the bulge in the parallel direction exceeds the gap width (Figure 9C).

The data from the moderately confined case were Fourier decomposed in order to quantitate the asymmetry of the growth rates. The profiles were fit to the following equations:

$$R_{||} = \sum_n (a_{||n} \sin(2\pi nz/L) + b_{||n} \cos(2\pi nz/L)) + \langle R_{||}(t) \rangle$$

$$R_{\perp} = \sum_n (a_{\perp n} \sin(2\pi nz/L) + b_{\perp n} \cos(2\pi nz/L)) + \langle R_{\perp}(t) \rangle$$

We find that the largest contributions are made by the n = 1 modes of $a_{||}$ and $a_{\perp}$. This is expected because it describes a growing sinusoidal distortion. Note that in the logarithmic plot of Figure 10 the difference between the parallel and perpendicular components of the primary mode is small. As the distortion increases, Figure 9 qualitatively shows that the thread becomes increasingly different from a simple sine wave. This behavior is captured in the n = 2 component. Surprisingly (see figure), it is found that, although the first-harmonic contribution is largest, the growth rate of the second harmonic (of the cosine term) was faster than the first harmonic (sine term). Also, while the amplitude of the first harmonic (sine) was larger in the plane parallel to the wall, the second harmonic was larger in the plane perpendicular to the wall. This behavior indicates that distortion from a pure sine wave is stronger in the confinement direction than in the unconfined direction, which is intuitively reasonable.

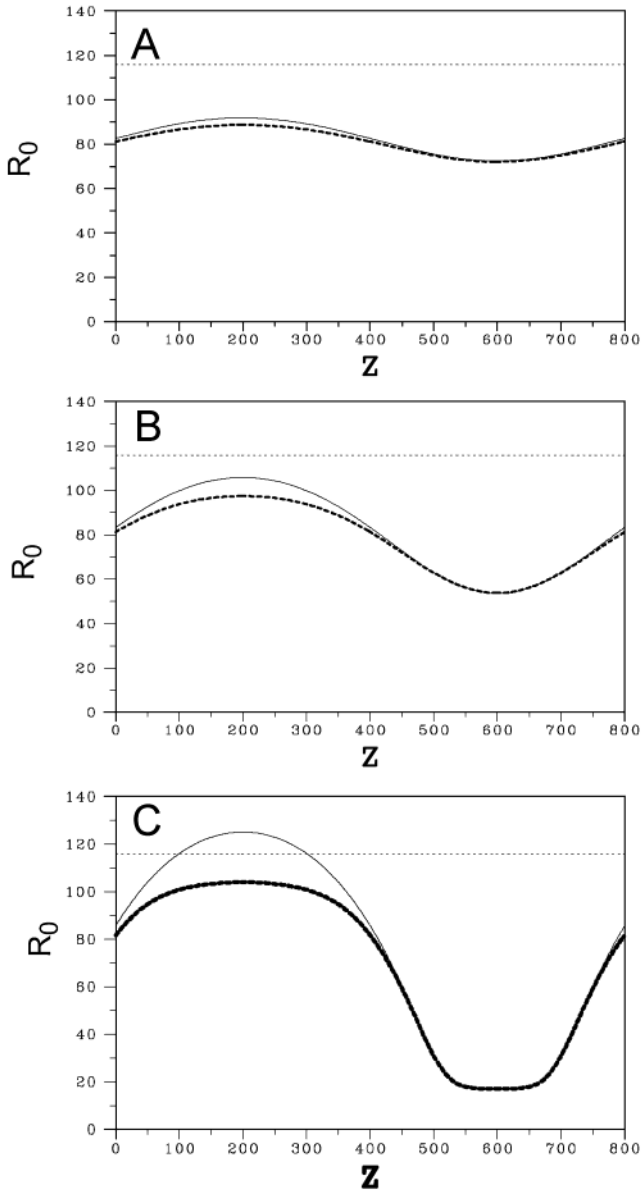

Figure 9. Profiles of the growing fluctuation for the moderately confined thread as it breaks up. The solid curve is the profile in the x (unconfined) direction, and the dashed curve is in the y confined direction. The dashed line at 117 shows the position of the confining wall in the y direction. (A) t = 73.9, (B) 77.1, and (C) 78.6.

Finally, in regard to the issue of thread stability for the highly confined case, we note that in the previous experiment by Migler[10] where p = 1, the critical confinement for stability was $H/D_0 = 0.83 \pm 0.15$. The critical confinement in the viscous mismatched experiments described with p = 0.25 is $H/D_0 = 1.3 \pm 0.1$. It is intuitively reasonable that the higher viscosity of the matrix prevents it from being squeezed out, and thus the geometrical confinement has a stronger impact on the thread. In the simulations of the viscous matched case, we find that the critical confinement occurs at H/D_0 = 1.2 which is larger than expected when compared to the prior results of Migler. However, because of the computational constraints described earlier, we view the critical value of H/D_0 as determined by simulation to be an upper bound to the actual value.

For the purposes of comparison to experiment, we utilize numerical data from the viscosity mismatched

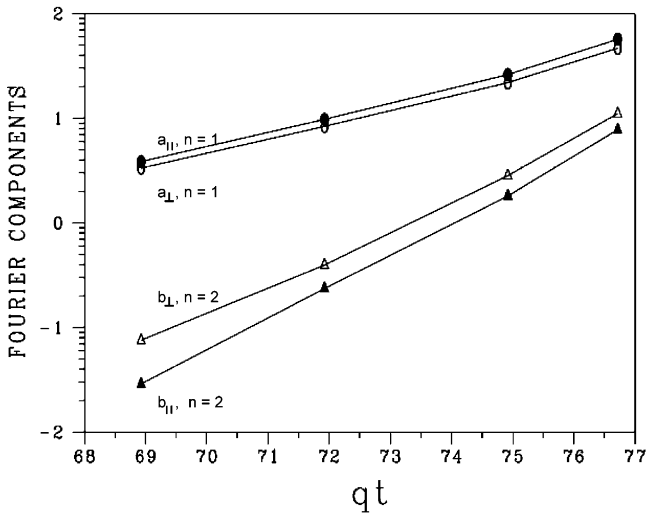

Figure 10. Major components of the Fourier transform of the profiles in the moderately confined case. See text for details.

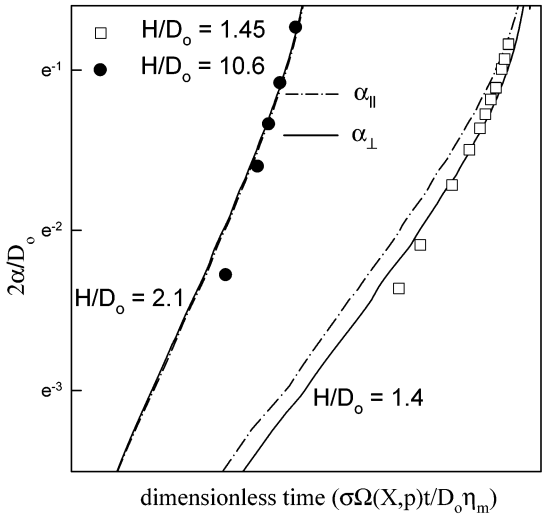

Figure 11. Comparison between the experimental (discrete points: same data with Figure 4; viscosity ratio $p = 0.25$) and computer-simulated (solid and dashed lines, viscosity ratio $p = 1$) dimensionless thread distortion amplitude, $2\alpha/D_0$, as a function of dimensionless time for two different H/D_0 ratios, showing consistency between the slopes measured experimentally and through the lattice−Boltzmann method.

simulations. Returning to Figure 3, we construct a plot of dimensionless apparent volume (defined previously) as a function of the amplitude of the distortion. The solid line is the simulation result, and the discrete data points are from the experiments. For the unconfined data, in the case of the experiments we used $H/D_0 = 10.6$ and for the simulations we used $H/D_0 = 2.1$ (for reasons of computational time). However, both these conditions correspond to essentially unconfined behavior. For the case of $H/D_0 = 2.1$, we see that $V'_{app} = 1$, indicating axisymmetric growth, whereas for the case of $H/D_0 = 1.4$, the upward trend of the curve indirectly indicates the nonaxisymmetric growth. This is quite similar to that observed experimentally, indicating the qualitative agreement between the two approaches.

Next, we extract data from the simulations that is contained in the (y) direction. In Figure 11, the calculated dimensionless amplitudes under two ratios of the gap width to the initial thread diameter (H/D_0) are presented as a function of time (solid curves) with the experimental data of Figure 4 included as well (discrete points). For the unconfined data, in the case of the experiments we used $H/D_0 = 10.6$, and for the simulations we used $H/D_0 = 2.1$ for reasons of computational time. But both these conditions correspond to essentially unconfined behavior. Note that the experimental data are shifted horizontally to achieve the best fit, and so the comparison between experiment and simulation is relevant to the growth rate rather than the absolute time of the experiment. Again, we see that the simulation results qualitatively agree with the experimental results. The amplitude growth rate decreases with decreasing H/D_0. For $H/D_0 = 2.1$, the amplitudes in the parallel and perpendicular directions are nearly equal, showing that the thread is axisymmetric. For the case of $H/D_0 = 1.4$, we find that the growth rate is strongly suppressed at early times but increases with time. Also, we find that the growth is no longer axisymmetric. The amplitude in the fluctuation in the direction perpendicular to the wall is reduced relative to that in the parallel direction. This is similar to the experimental result in the confined case. The other noteworthy feature is that the ratio of $\alpha_{||}$ (amplitude parallel to the plate) to $\alpha_{\perp}$ (amplitude perpendicular to the plate) ratio is approximately constant during the growth of the instability. This finding, along with the observation that the necks are circular, is used in the next section.

Surface Area Calculations. To understand the increase in wavelength (λ) and the decrease in the growth rate of the instability in the moderately confined regime, we turn to a simple (in principle) calculation of the surface area of a thread when the fluctuation is no longer axisymmetric but somewhat flattened as depicted in Figure 1. The simplifying assumption behind this calculation is that the principal effect of the complex hydrodynamic interactions between the thread and the confining wall is to cause a fluctuation that is nonaxisymmetric. The cross section of the thread is no longer circular, but rather ellipsoidal at the bulges. We consider the nonaxisymmetry to be a fixed feature of the instability and then calculate the critical wavenumber X_c.

We assume that the surface equation of our nonaxisymmetric sinusoidal thread is expressed by the following equation:

$$r(\theta,z) = \left[\left(\frac{\cos(\theta)}{r_{||}(z)}\right)^2 + \left(\frac{\sin(\theta)}{r_{\perp}(z)}\right)^2\right]^{-0.5} \tag{6}$$

where

$$r_{||}(z) = r_{||}' + \alpha_{||}\sin\left(\frac{2\pi}{\lambda}z\right) \tag{7}$$

$$r_{\perp}(z) = r_{\perp}' + \alpha_{\perp}\sin\left(\frac{2\pi}{\lambda}z\right) \tag{8}$$

Equation 6 describes that the cross section at the maximum perimeter ($z = \lambda$) is an ellipse with a major axis of $r_{||}' + \alpha_{||}$ and a minor axis of $r_{\perp}' + \alpha_{\perp}$, as depicted in Figure 1.

Here, we assume that the amplitude growth toward the wall, $\alpha_{\perp}$, is

$$\alpha_{\perp} = f\alpha_{||} \tag{9}$$

and f can be defined as a degree of flattening. Equation 9 is supported by the observation described in the last

section that $\alpha_\perp/\alpha_\parallel$ is approximately constant during the growth of the instability. Next, we calculate the surface area of the nonaxisymmetric sinusoidal thread as a function of the dimensionless wavenumber, the degree of flattening, and the relative amplitude.

Utilizing volume conservation of the thread during nonaxisymmetric growth and assuming that the cross section at the neck is circular ($r_\parallel' - \alpha_\parallel = r_\perp' - \alpha_\perp$) (as found in the simulations), we obtain the following relations:

$$r_\parallel' = \frac{(1-f)\alpha_\parallel + \sqrt{4R_0^2 + (f^2 - 4f + 1)\alpha_\parallel^2}}{2} \quad (10)$$

$$r_\perp' = \frac{-(1-f)\alpha_\parallel + \sqrt{4R_0^2 + (f^2 - 4f + 1)\alpha_\parallel^2}}{2} \quad (11)$$

Then surface area of the thread per λ is as follows:[25]

$$S = \int_0^\lambda \int_0^{2\pi} \sqrt{r(\theta,z)^2 + \left(\frac{\partial r(\theta,z)}{\partial \theta}\right)^2} \sqrt{1 + \left(\frac{\partial r(\theta,z)}{\partial z}\right)^2}\, \partial\theta\, \partial z \quad (12)$$

Equation 12 cannot be integrated analytically. However, its first and second derivative with respect to $\alpha_\parallel$ at 0 can be obtained analytically. The results are as follows:

$$\left.\frac{\partial S}{\partial \alpha_\parallel}\right|_{\alpha_\parallel=0} = 0 \quad (13)$$

$$\left.\frac{\partial^2 S}{\partial \alpha_\parallel^2}\right|_{\alpha_\parallel=0} = \frac{2\lambda}{\pi R_0}[(7 - 22f + 7f^2) + X^2(3 + 2f + 3f^2)] < 0 \quad (14)$$

Equation 14 is a necessary condition for the distortion growth.

In Figure 12, we present the surface area of the sinusoidal thread divided by that of initial thread vs the amplitude at two different values of f. For the axisymmetric case of $f = 1$ (Figure 12A), we plot the normalized surface area for three different values of X. We see that only distortions with $X < 1$ cause a decrease in surface area, as discussed previously, i.e., $X_c(f=1) = 1$. In Figure 12B, making $f < 1$ captures the nonaxisymmetric growth of the thread, and we see its effect on surface area is different. We find that the critical wavenumber is shifted. For $f = 0.5$, we now have X_c (f=0.5) = 0.687. We present a plot of the critical wavenumber ($2\pi R_0/\lambda_c$) vs f in Figure 13. The critical wavenumber decreases with decreasing f. Thus, the wavelength increases as a result of confinement in a manner similar to the experiment. It is interesting that the critical wavenumber becomes zero below a certain value of f ($\approx$0.36). That may explain our experimental result that the thread placed between a gap whose size slightly larger than the thread diameter does not show the distortion growth at all. The dominant wavenumber, X_m, at which the amplitude grows fastest will also decrease as the critical wavenumber decreases. Experimentally, we observe X_m rather than X_c.

Intuitively, we can understand the above result on the basis of eqs 4 and 5. The reduction of surface area upon the growth of a fluctuation occurs in an axisymmetric thread because the average radius (denoted by R' in Figure 1) of the thread must decrease in order to conserve volume. In the nonaxisymmetric case, this decrease in the average radius is less, and so the increase in surface area due to the contour length increase becomes dominant. Note that f cannot be predicted from the present analysis for a given degree of confinement and viscosity ratio. Our primary goal in the surface area calculations is to show that forcing the growth to be nonaxisymmetric can cause the wavelength to increase and to reduce the driving force for breakup. We note that other choices for the shape of the nonaxisymmetric thread are possible other than that described. For example, we also considered a shape wherein the inflection point was circular and both the bulges and necks were elliptical. This too produced a similar result with a slightly smaller value of f where the critical wavenumber becomes zero. While our choices of axisymmetric growth is consistent with experiment and simulation, a more rigorous approach would utilize a calculus of variations coupled with knowledge of the initial grow rates in the parallel and perpendicular directions.

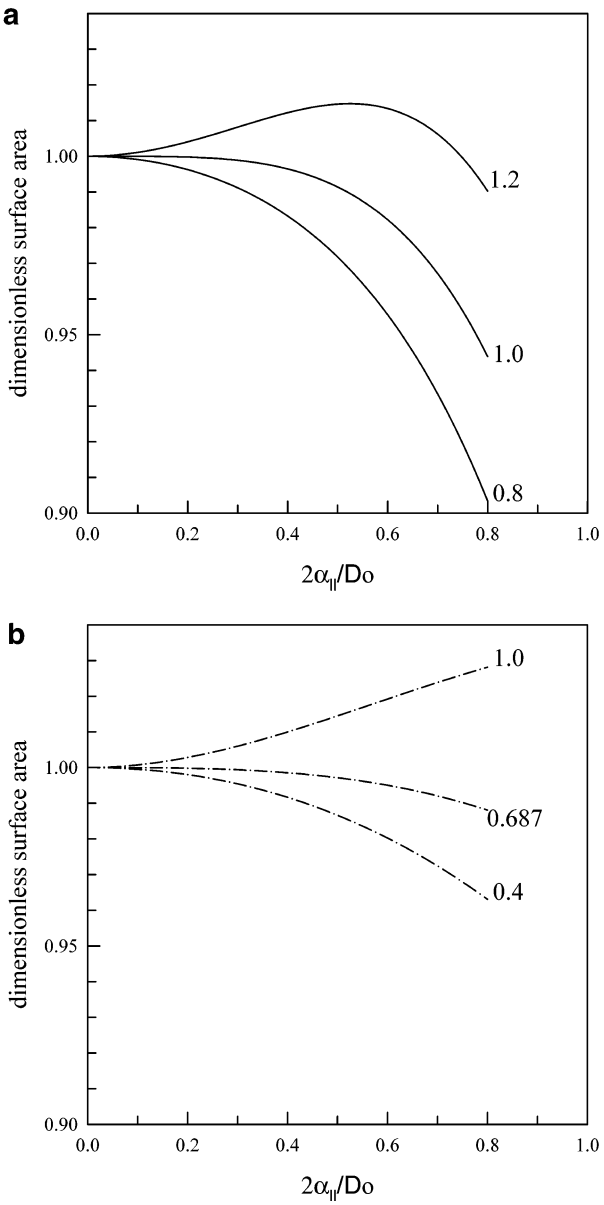

Figure 12. Normalized surface area of a nonaxisymmetric sinusoidal cylinder as a function of relative amplitude. Numbers in each curve represent dimensionless wavenumbers. (a) $f = 1$, (b) $f = 0.5$.

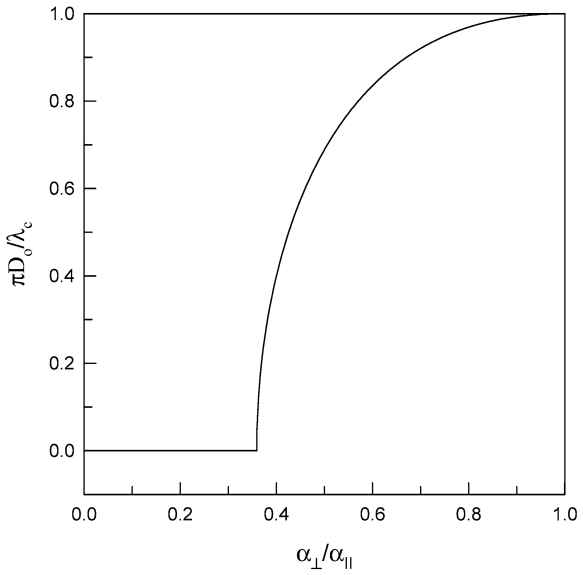

Figure 13. Critical dimensionless wavenumber ($\pi D_0/\lambda_c$) vs $\alpha_+/\alpha_{||}$. λ_c is a minimum wavelength, which allows the distortion growth.

Conclusion

We find that the behavior of the distortion growth when the matrix fluid is confined between parallel plates is much different from that in the unconfined regime. An initially axisymmetric cylindrical thread transforms into a nonaxisymmetric thread in the confined regime while that at the unconfined regime maintains an axisymmetric shape. The rate of the distortion growth and the observed dimensionless wavenumber ($2\pi R_0/\lambda$) in the confined regime is much smaller than that for the unconfined regime. Below a certain ratio of gap width/thread diameter, the thread does not exhibit a distortion growth at all but is quite stable for a long period, if not indefinatley. The lattice−Boltzmann simulations confirm the physical assumptions made in the surface area analysis; in particular, they indicate that the necks are circular while the bulges are nonaxisymmetric as quantified by the Fourier decomposition relations. A simple calculation of the surface area of the nonaxisymmetric sinusoidal thread indicates that the increase in wavelength of the distortion in the confined regime is caused by the increase in the minimum wavelength required in order to have a net decrease in surface area. Finally, we note that the construction of a linear stability analysis for this nonaxisymmetric case would greatly enhance our understanding of this intriguing phenomenon.

Acknowledgment. We acknowledge Jack Douglas for important discussions.

References and Notes

(1) Rayleigh, Lord *Proc. R. Soc. London* **1879**, *29*, 71.
(2) Tomotika, S. *Proc. R. Soc. London, Ser. A* **1935**, *150*, 322.
(3) Paul, D. R.; Newman, S. *Polymer Blends*; Academic Press: New York, 1978.
(4) Hansen, S.; Peters, G. W. M.; Meijer, H. E. H. *J. Fluid Mech.* **1999**, *382*, 331.
(5) Kwak, S.; Pozrikidis, C. *Int J. Multiphase Flow* **2001**, *27*, *1*.
(6) Pozrikidis, C. *J. Fluid Mech.* **2000**, *405*, 211.
(7) Miguel, M. S.; Grant, M.; Gunton, *J. D. Phys. Rev. A* **1985**, *31*, 1001.
(8) Goren, S. L. *J. Colloid Sci.* **1964**, *19*, 81.
(9) Newhouse, L. A.; Pozrikidis, C. *J. Fluid Mech.* **1992**, *242*, 193.
(10) Migler, K. B. *Phys. Rev. Lett.* **2001**, *86*, 1023.
(11) Sung, L.; Karim, A.; Douglas, J. F.; Han, C. C. *Phys. Rev. Lett.* **1996**, *76*, 4368.
(12) Nakanishi, H.; Fisher, M. E. *J. Chem. Phys.* **1983**, *78*, 3279.
(13) Cho, K. W. L.; Jeon, H. K.; Park, C. E.; Kim, J.; Kim, K. U. *Polymer* **1996**, *37*, 1117.
(14) Elemans, P. H. M.; Janssen, J. M. H.; Meijer, H. E. H. *J. Rheol.* **1990**, *34*, 1311.
(15) Elmendorp, J. J. *Polym. Eng. Sci.* **1986**, *2*, 418.
(16) Xing, P.; Bousmina, M.; Rodrigue, D.; Kamal, M. R. *Macromolecules* **2000**, *33*, 8020.
(17) Certain equipment, instruments or materials are identified in this paper in order to adequately specify the experimental details. Such identification does not imply recommendation by the National Institute of Standards and Technology nor does it imply the materials are necessarily the best available for the purpose.
(18) Martys, N. S.; Douglas, J. F. *Phys. Rev. E* **2001**, *63*, 031205.
(19) Chen, H.; Chen, S. Y.; Matthaeus, W. H. *Phys. Rev. A* **1992**, *45*, R5339.
(20) Shan, X.; Doolen, G. *Phys. Rev. E* **1996**, *54*, 3616.
(21) Martys, N. S.; Chen, H. *Phys. Rev. E* **1996**, *53*, 743.
(22) Shan, X.; Chen, H. *Phys. Rev. E* **1993**, *47*, 1815.
(23) Luciani, A.; Champagne, M. F.; Utracki, L. A. *Macromol. Symp.* **1998**, *126*, 307.
(24) Son, Y. *Polymer* **2001**, *42*, 1287.
(25) Pearson, C. E. *Handbook of Applied Mathematics*, 2nd ed.; Van Nostrand Reinhold Co.: New York, 1983; Chapter 2, p 102.

MA0343986